Original Article

Institution of MECHANICAL ENGINEERS
Journal of MATERIALS: DESIGN AND APPLICATIONS

Damping in beams using viscoelastic layers

Proc IMechE Part L:
J Materials: Design and Applications
2015, Vol. 229(2) 117–125

DOI: 10.1177/1464420713500748
pil.sagepub.com
SAGE

K Kishore Kumar[1], Y Krishna[1] and P Bangarubabu[2]

Abstract

Various types of sandwich beams with viscoelastic cores are currently used in aerospace and automotive industries, indicating the need for simple methods describing the dynamics of these complex structures. In order to understand the effectiveness of the sandwich structures, the dynamics of bare beam with unconstrained and constrained viscoelastic layers are investigated in this study. The viscoelastic layer is bonded uniformly on the beam. The effects of distributed viscoelastic layer treatment on the loss factors are studied. From the experiments it is observed that beams with constrained viscoelastic layer provide higher loss factors than those with unconstrained layer. The dynamics of sandwich beams is modeled using Euler and Bernoulli beam theory. Frequency-dependent Young's modulus and loss factors are considered in the model of viscoelastic material. The predicted Eigen frequencies obtained from the model are compared with the experimental results for two viscoelastic materials with aluminum base material. Frequency response functions are obtained from the finite element model and compared with experimental results for harmonic input. Reductions in vibration amplitudes for two viscoelastic materials (EAP-2 and EAP-43) are also compared. Based on the experimental results, it has been observed that the loss factors of EAP-43 are higher than that of EAP-2.

Keywords

Unconstrained layer, constrained layer, loss factor, frequency response function, energy-absorbing polymer, viscoelastic layer

Date received: 8 February 2013; accepted: 16 July 2013

Introduction

Noise and vibration control is a major concern in several industries such as aerospace and automobiles. The reduction of noise and vibration is a major requirement for performance and customer satisfaction. Passive damping technology using viscoelastic materials (VEMs) is generally used to control vibrations. The growing use of such structures has motivated many authors to study sandwich structures. Damping treatment using constrained and unconstrained layers using VEM is a common method to control vibrations. In unconstrained layer damping, the viscoelastic layer is glued to the bare beam. The dissipation of energy in unconstrained layer is by means of extension and compression of the viscoelastic layer. In constrained layer damping, the VEM is glued between two metallic sheets. Flexural vibrations causes shear strain in the core, which dissipates energy and thereby reduces vibrations. Adding a VEM to a structure and predicting response is a challenging task. This is because the properties of VEM including the Young's modulus and loss factors, vary significantly as a function of frequency and temperature. The fundamental work in this field was pioneered by Ross, Ungar and Kerwin (RKU),[1] who used a three-layer model to predict damping in plates with constrained layer damping treatment. Kerwin[2] was the first to present a theoretical approach of damped thin structures with a constrained viscoelastic layer. He observed that the energy dissipation mechanism in the constrained core is due to its shear motion. He presented the first analysis of the simply supported beam using a complex modulus to represent viscoelastic core. Several authors, DiTaranto[3], Mead and co-workers[4,5] and Rao,[6] extended Kerwin's work. Nakra[7–9] has carried out an excellent literature review on the topic, dealing with vibration control with VEMs. Johnson and Kienholz[10] used

[1]Defence Research and Development Laboratory, Hyderabad, Andhra Pradesh, India
[2]Department of Mechanical Engineering, National Institute of Technology, Warangal, Andhra Pradesh, India

Corresponding author:
K Kishore Kumar, Department of Mechanical Engineering, National Institute of Technology, Warangal 506004, Andhra Pradesh, India.
Email: kalahasti_kishorekumar@yahoo.com

three-dimensional bricks in their model. Johnson used solid elements (Hexa8) for the viscoelastic core and quadrilateral thick shell elements (quad4) with offsets for the face sheets. Hughes and co-workers[11,12] and Lesieutre and Bianchini[13] presented a time-domain response of structures containing viscoelastic components. Torvik and Runyon[14] studied the loss factor of plates with CLD treatment for various boundary conditions. Cortes and Elejabarrieta[15] analyzed the dynamic behavior of unconstrained layer damping with a thick viscoelastic layer. Modeling of sandwich beams using complex modulus approach is discussed by Barbosa and Farage.[16] For constrained layer beam, shear effect in the core is modeled by Amichi and Atalla[17] and Navin Kumar and Singh.[18] This study deals with modeling of unconstrained and constrained layer beam using Euler–Bernoulli theory for base excitation considering the frequency-dependent Young's modulus and loss factor of viscoelastic layer and validation with experimental results. Two VEMs are studied to understand their composite loss factors in unconstrained and constrained layer damping treatment. For constrained layer beam, shear effect in the core as studied by Navin Kumar and Singh[18] is also modeled and it is found that there is little increase in loss factors compared with Euler–Bernoulli model for thickness considered in this study.

Frequency-dependent stiffness and damping property of the viscoelastic layer are considered for predicting the response spectrum. Complex Young's modulus of VEM is computed using Young's moduli and loss factors obtained from dynamic mechanical analyzer (DMA). Finite element (FE) model is developed for base excitation with cantilever boundary condition and the model is validated with experimental results.[19] During extraction of eigen values and eigen vectors, the real component of global stiffness matrix of the sandwich beam is used. Frequencies are changed iteratively and at each frequency, the real component of stiffness matrix is changed and the response corresponding to the excitation frequency is stored and frequency–response functions (FRFs) are calculated. The imaginary part of stiffness matrix of VEM along with experiment loss factors of bare beam are used to extract theoretical composite loss factors for unconstrained and constrained layer beams and validated with experimental loss factors.

This article is organized as follows. In the next section, FE formulation and state space technique for extraction of FRF is discussed and this is followed by details on the experimental setup and test details. Test results and discussion are presented in the next section and some important conclusions are presented in the last section.

FE formulation for sandwich beams

The sandwich beam is modeled as Euler–Bernoulli beam to evaluate the dynamic properties.[20] The beam is discretized using two-noded beam elements, with two degrees of freedom (DOF), translation and rotation at each node. FE code is developed in MATLAB®. Ninety-six elements are used to discretize the beam. The equations of motion with harmonic excitation for the discretized beam can be written as

$$[M]\{\ddot{w}\} + [K^*]\{w\} = f(t) \tag{1}$$

where [K*] is global complex stiffness matrix, w is the displacement vector and [M] is the global mass matrix.

$$[K]^* = [K]^R + [K]^I \tag{2}$$

where $[K]^R$ is real part of the complex global stiffness matrix and $[K]^I$ is the imaginary part of complex global stiffness matrix.

The element equivalent complex stiffness matrix for the two-node sandwich beam element is given as

$$[k^e]^*_{eq} = \frac{(EI)_{eq}}{L_e^3}\begin{bmatrix} 12 & 6L_e & -12 & 6L_e \\ 6L_e & 4L_e^2 & -6L_e & 2L_e^2 \\ -12 & -6L_e & 12 & -6L_e \\ 6L_e & 2L_e^2 & -6L_e & 4L_e^2 \end{bmatrix} \tag{3}$$

where $(EI)_{eq} = E^*(f)\ I^v + E^b\ I^b$ is the equivalent EI distribution for the sandwich beam element, E*(f) and I^v are the complex Young's modulus and moment of inertia of sandwich beam, respectively, E^b and I^b are the Young's modulus and moment of inertia of base beam, respectively, and f is the frequency in hertz.

$$E^*(f) = E^v(f)(1 + i\eta(f)) \tag{4}$$

where $\eta(f)$ is the frequency-dependent loss factor of the VEM. The Young's modulus of VEM $E^v(f)$ can be represented by

$$E^v(f) = a_1 f^{b_1} + c_1 \tag{5}$$

and loss factor $\eta(f)$ can be represented by

$$\eta(f) = a_2 f^{b_2} + c_2 \tag{6}$$

where a_1, b_1, c_1, a_2, b_2 and c_2 are the constants obtained from the curve fit of measured data for the frequency-dependent Young's modulus and loss factors of the VEMs obtained using DMA results.

The element mass matrix of sandwich beam is given as

$$[m^e]_{eq} = \frac{m_e L_e}{420}\begin{bmatrix} 156 & 22L_e & 54 & -13L_e \\ 22L_e & 4L_e^2 & 13L_e & -3L_e^2 \\ 54 & 13L_e & 156 & -22L_e \\ -13L_e & -3L_e^2 & -22L_e & 4L_e^2 \end{bmatrix} \tag{7}$$

where m_e and L_e are the mass per unit length of sandwich beam and length of the element, respectively.

The effect of shift in the neutral axis of the sandwich beam due to the viscoelastic layer is found to be insignificant and it is not considered in this analytical model.

The resultant equation of motion for the sandwich beam after assembling the elemental equations can be written as

$$[M]\{\ddot{w}(t)\} + [C]\{\dot{w}(t)\} + [K]\{w(t)\} = \{0\} \tag{8}$$

where $[C] = \frac{K^I}{\omega}$, where K^I is the imaginary part of global complex stiffness matrix, ω is the angular frequency and is equal to $2\pi f$, $[K] = [K^R]$ is the real part of global stiffness matrix of sandwich beam.

For base excitation problem, equation (8) can be written as

$$\begin{bmatrix} M_{cc} & M_{cu} \\ M_{uc} & M_{uu} \end{bmatrix} \begin{Bmatrix} \ddot{w}_c(t) \\ \ddot{w}_u(t) \end{Bmatrix} + \begin{bmatrix} C_{cc} & C_{cu} \\ C_{uc} & C_{uu} \end{bmatrix} \begin{Bmatrix} \dot{w}_c(t) \\ \dot{w}_u(t) \end{Bmatrix} + \begin{bmatrix} K_{cc} & K_{cu} \\ K_{uc} & K_{uu} \end{bmatrix} \begin{Bmatrix} w_c(t) \\ w_u(t) \end{Bmatrix} = \begin{Bmatrix} 0 \\ 0 \end{Bmatrix} \tag{9}$$

where $w(x,t) = \{w_c(x,t) w_u(x,t)\}^T$, $w_c(x,t)$ is the constrained DOF and $w_u(x,t)$ is the unconstrained DOF. The subscript cc and uu represent constrained and unconstrained part of mass, damping and stiffness matrices. The unconstrained displacements can be decomposed into pseudo-static $\{W_s\}$ and dynamic parts $\{W_d\}$ as

$$\{w_u(x,t)\} = \{w_s(x,t)\} + \{w_d(x,t)\} \tag{10}$$

The pseudo-static displacements may be obtained from equation (9) by excluding the first two terms on the left-hand side of the equation and by replacing $\{w_u\}$ by $\{w_s\}$

$$\{w_s(x,t)\} = -[K_{uu}]^{-1}[K_{uc}]\{w_c(x,t)\} = [\alpha]\{w_c(x,t)\} \tag{11}$$

where $[\alpha] = -[K_{uu}]^{-1}\ [K_{uc}]$ is constant and dimensionless.

Substituting equation (11) in equation (10) implies

$$\{w_u(x,t)\} = [\alpha]\{w_c(x,t)\} + \{w_d(x,t)\} \tag{12}$$

Substituting equation (12) in equation (9), we get

$$\begin{bmatrix} M_{cc} & M_{cu} \\ M_{uc} & M_{uu} \end{bmatrix} \begin{Bmatrix} \ddot{w}_c \\ \alpha\ddot{w}_c + \ddot{w}_u \end{Bmatrix} + \begin{bmatrix} C_{cc} & C_{cu} \\ C_{uc} & C_{uu} \end{bmatrix} \times \begin{Bmatrix} \dot{w}_c \\ \alpha\dot{w}_c + \dot{w}_u) \end{Bmatrix} + \begin{bmatrix} K_{cc} & K_{cu} \\ K_{uc} & K_{uu} \end{bmatrix} \begin{Bmatrix} w_c \\ \alpha w_c + w_u \end{Bmatrix} = \begin{Bmatrix} 0 \\ 0 \end{Bmatrix} \tag{13}$$

This implies that

$$[M_{uc}]\{\ddot{w}_c\} + [M_{uu}]\{\alpha w_c + \ddot{w}_d\} + [C_{uc}]\{\dot{w}_c\} + [C_{uu}]\{\alpha\dot{w}_c + \dot{w}_d\} + [K_{uc}]\{w_c\} + [K_{uu}]\{\alpha w_c + w_d\} = \{0\} \tag{14}$$

$$[M_{uu}]\{\ddot{w}_d\} + [C_{uu}]\{\dot{w}_d\} + [K_{uu}]\{w_d\} = -\{[M_{uc}] + [M_{uu}][\alpha]\}\{\ddot{w}_c\} - \{[C_{uc}] + [C_{uu}][\alpha]\}\{\dot{w}_c\} - \{[K_{uc}] + [K_{uu}][\alpha]\}\{w_c\} \tag{15}$$

For input base acceleration problems, the two terms corresponding to the dynamic displacements and velocities are neglected. Hence, equation (15) becomes

$$[M_{uu}]\{\ddot{w}_d\} + [C_{uu}]\{\dot{w}_d\} + [K_{uu}]\{w_d\} = -\{[M_{uc}] + [M_{uu}][\alpha]\}\{\ddot{w}_c\} \tag{16}$$

The right side of equation (16) is the base acceleration input

$$\gamma = -[M_{uc}] + [M_{uu}][\alpha] \tag{17}$$

From modal analysis approach, the response vector, $w_d(x,t)$ is given as

$$\{w_d(x,t)\} = [P]\{q_m(t)\} \tag{18}$$

where $[P]$ is the modal matrix and $\{q_m(t)\}$ is the modal response vector. The modal matrix can be obtained by solving the eigenvalue problem as

$$\{[K_{uu}] - [M_{uu}]\omega^2\}\{P\} = \{0\} \tag{19}$$

By transforming the equations of motion of equation (16) into the modal co-ordinates using equation (18), we can write

$$[P]^T[M_{uu}][P]\{\ddot{q}_m(t)\} + [P]^T[C_{uu}][P]\{\dot{q}_m(t)\} + [P]^T[K_{uu}][P]\{q_m(t)\} = [P]^T[\gamma]\{\ddot{w}_C(t)\} \tag{20}$$

This equation can be further simplified as

$$[M_m]\{\ddot{q}_m(t)\} + [C_m]\{\dot{q}_m(t)\} + [K_m]\{q_m(t)\} = [\gamma_m]\{\ddot{w}_C(t)\} \tag{21}$$

where $[M_m] = [P]^T[M_{uu}][P]$ is the modal mass matrix, $[K_m] = [P]^T[K_{uu}][P]$ is the modal stiffness matrix, $[C_m] = [P]^T[C_{uu}][P]$ is the modal damping matrix and $[\gamma_m] = [P]^T\{\gamma\}$ is the modal force vector.

Equation (21) is the uncoupled dynamic equation of the beam and for the i^{th} mode and it can be written as

$$m_{m\,i}\ddot{q}_{mi} + c_{mi}\dot{q}_{mi} + k_{mi}q_{mi} = \gamma_{mi}\{\ddot{w}_c(t)\} \tag{22}$$

Let $u(t) = \ddot{w}_c(t)$

State space formulation

Equation (22) is used to develop the state space model of the beam.[21] Considering the state vectors as

$$\{z_1(t)\} = \{q_{mi}(t)\} \tag{23a}$$

$$\{z_2(t)\} = \{\dot{q}_{mi}(t)\} \tag{23b}$$

Using equation (23), equation (22) can be written as

$$\begin{Bmatrix} \dot{z}_1(t) \\ \dot{z}_2(t) \end{Bmatrix} = \begin{bmatrix} 0 & 1 \\ -m_{mi}^{-1}k_{mi} & -m_{mi}^{-1}c_{mi} \end{bmatrix} \begin{Bmatrix} z_1(t) \\ z_2(t) \end{Bmatrix} + \begin{bmatrix} 0 \\ F_{mi} \end{bmatrix} \{u(t)\} \tag{24}$$

where F_{mi} indicates the participation factor for particular mode.

This equation can be simplified as

$$\{\dot{z}(t)\} = [A]\{z(t)\} + [B]\{u(t)\} \tag{25}$$

where [A] is the state matrix and [B] is the input matrix.

Considering the accelerometer response, we can write

$$\{\ddot{q}_{mi}(t)\} = [0 \quad 1]\{\dot{z}(t)\} = [\beta]\{\dot{z}(t)\} \tag{26a}$$

where $[\beta] = [0\ 1]$.

Substituting equation (25) into equation (26a), we get

$$\{\ddot{q}_{mi}(t)\} = [\beta][A]\{z(t)\} = [B]\{u(t)\} \tag{26b}$$

Using equations (26b) and (25), the modal transfer functions can be evaluated as

$$[H_{mi}(s)] = [\beta][A][sI - A]^{-1}[B] + [\beta][B] \tag{27}$$

The overall transfer functions for first three modes at a tip of the beam can be found as

$$[H(s)]_i = \sum_{i=1}^{3} \{P\}_i[(H_{mi}(s))] \tag{28}$$

Mode summation method is used to calculate the overall response of the beam at a particular location. The response at a particular location is calculated for a given harmonic input.

Experimental damping ratios are used for aluminum beam and constrained layer in the FE model. The imaginary part of the modal stiffness matrix is used for computing damping matrix of VEM. Damping matrix of layer beam is obtained by adding the aluminum beam modal damping ratio obtained from experiments and viscoelastic damping matrix.

Frequency-dependent properties

Two VEMs, EAP-2 and EAP-43, are evaluated for their Young's modulus and loss factor characteristics. The variation of Young's modulus and loss factor with frequency for both the materials is obtained from DMA at room temperature and is shown in Figure 1(a) and (b), respectively. The corresponding constants are obtained using equations (5) and (6) and are given in Table 1. The polymers used in EAP-2 and EAP-43 are nitrile butadiene rubber and polyvinyl chloride blend. The two materials differ in terms of type of filler used. EAP-2 has titanium dioxide as the pigment and semi-reinforced filler, while EAP-43 has carbon black as reinforced filler. The rubber matrix–filler interaction is high in carbon black and as a result, the rubber molecules get incorporated and immobilized in the carbon black structure. Due to carbon black filler, EAP-43 has higher Young's modulus and loss factor, which is due to inter-particle friction and reversible breakage of carbon particle structure on application of strain.

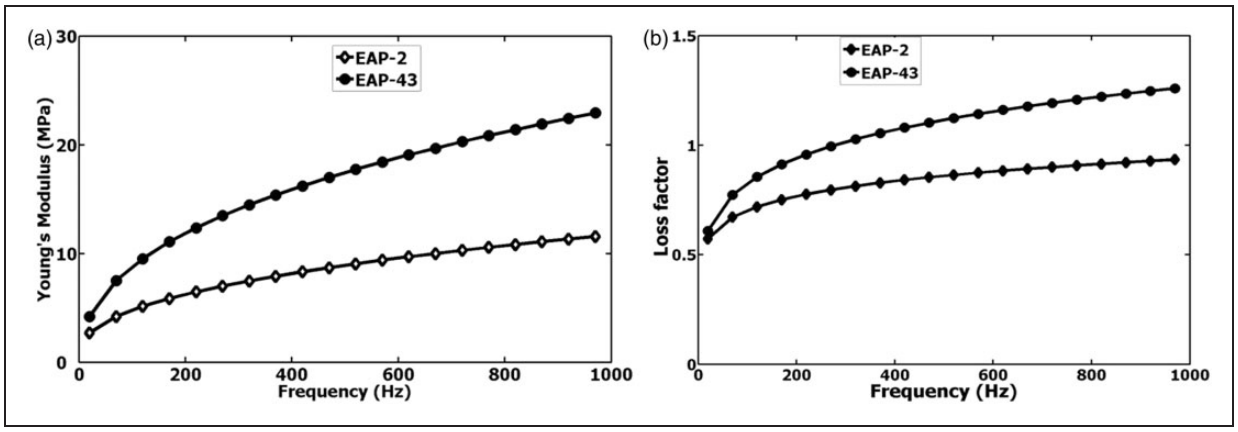

Figure 1. (a) Variation of Young's modulus with frequency and (b) variation of loss factor with frequency.

Experimental setup

An aluminum beam of 300 mm length, 30 mm width and 5.8 mm thickness is used to carry out experiments in cantilever boundary condition. The Young's modulus and density of aluminum beam is 70 GPa and 2800 kg/m^3, respectively. Two VEMs (EAP-2 and EAP-43) are studied to understand composite loss factors in unconstrained and constrained layer aluminum beam. The dimensions of the VEM are 290 mm length, 30 mm width and 1 mm thickness and the density of EAP-2 and 43 are 1220 kg/m^3 and 1260 kg/m^3, respectively. The test setup of the sandwich beam with unconstrained and constrained viscoelastic core is shown in Figure 2. The unconstrained and constraining layers remained free at both ends. Epoxy-based adhesive is used to glue the viscoelastic layer to the aluminum beam and the viscoelastic layer to the constraining layer beam. Aluminum beam of 290 mm length, 30 mm width and 1 mm thickness is used as constraining layer beam. The thickness of the viscoelastic layers is 1 mm in both unconstrained and constrained layer beam. The treated test beam is rigidly clamped at its base in between two solid plates to simulate cantilever boundary conditions, as shown in Figure 3(a). Experiments are conducted on aluminum base beams with two VEMs (EAP-2 and EAP-43) for unconstrained and constrained layer configuration. In all experiments, only the base beam is clamped, as shown in Figure 2. Electrodynamic shaker is used to carry out experiments. An accelerometer kept on the clamping plate measures the base acceleration and the other accelerometer mounted at the tip of the beam measures the response. PC-based LMS controller and data acquisition system is used to provide harmonic acceleration input to the shaker. The beam is tested for frequency band of 20–1000 Hz with a sweep rate of 1 Hz/s at off resonance and 0.01 Hz/s around resonance. The time domain base acceleration input

Table 1. Constants of EAP-43 and EAP-2 obtained from curve fit of DMA data.

	Viscoelastic material	
Constants	EAP-43	EAP-2
a_1	1.599×10^6	1.24×10^6
b_1	0.3933	0.4179
c_1	-9.86×10^5	1.249×10^5
a_2	0.4012	0.436
b_2	0.174	0.1189
c_2	−0.0679	−0.04848

DMA: dynamic mechanical analyzer.

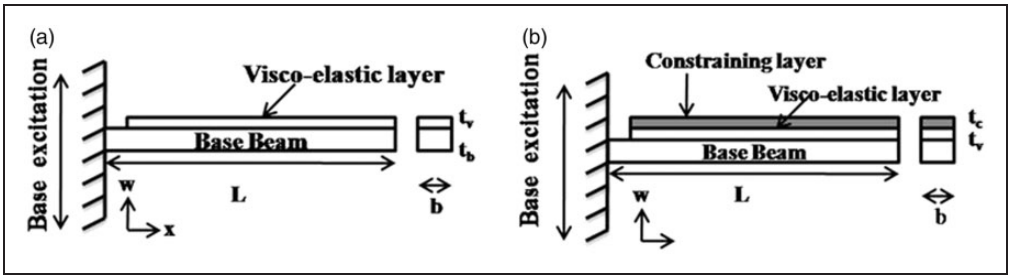

Figure 2. (a) Sandwich beam with unconstrained viscoelastic layer (L is the length of base beam, 300 mm; b is the width of base beam, 30 mm; length of constraining layer, 290 mm and length of viscoelastic layer, 290 mm) and (b) Sandwich beam with constrained viscoelastic layer (t_b is the thickness of base beam, 5.8 mm; t_v is the viscoelastic layer thickness, 1 mm and t_c is thickness of constraining layer, 1 mm).

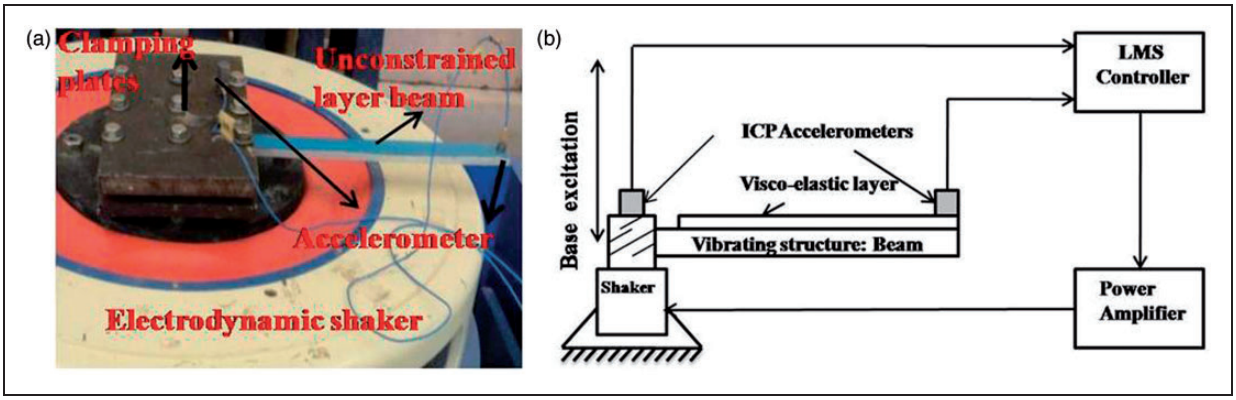

Figure 3. (a) Unconstrained layer beam attached to electro-dynamic shaker and (b) schematic of the experimental setup.

and response at the tip of the beam is transformed to frequency domain using fast Fourier transform.

Results and discussion

Aluminum beam

Figure 4 shows the comparison of the FRF obtained from the FE model and experiment at the tip of aluminum beam. Table 2 shows the comparison of FE and experimental natural frequencies and the results match very well. The modal damping ratio's for the first three natural frequencies calculated from the experimental FRF using half-power technique[22] are 0.006, 0.0065 and 0.0073, respectively. The amount of damping present in the aluminum beam is very low and is attributed to structural damping of aluminum beam and the energy dissipated due to friction in clamping supports.

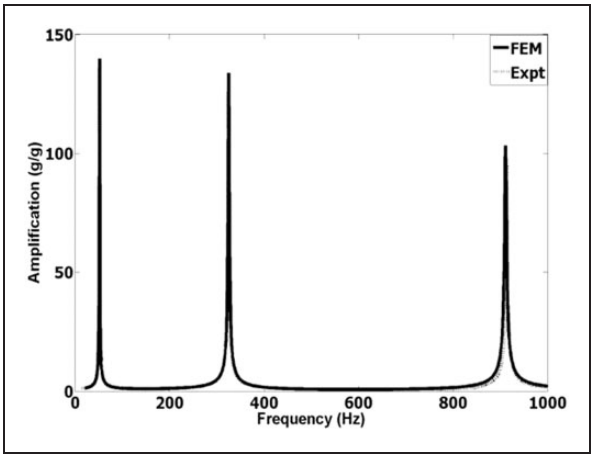

Figure 4. Comparison of FRF at the tip of the aluminum beam.
FRF: frequency–response function.

Beam with unconstrained viscoelastic layer sandwich beam (EAP-2 and EAP-43)

From Figure 5(a) and (b), it is seen that the FRF obtained from FE and experiments compare very well for unconstrained layer of 1 mm thickness for EAP-2 and EAP-43, respectively, and are given in Table 3 along with comparison of loss factors. The results are fairly matching and the difference in natural frequencies between theory and experiment can be attributed to the overall error of the measurement chain in frequency and amplitude measurement and it is found to be 1%. Comparison of amplification factors are made by considering the respective first, second and third modes of bare beam as 0 dB. An attenuation of 21, 37 and 50 dB in amplitudes is observed for EAP-2. For EAP-43, an amplitude attenuation of 21, 38 and 56 dB are observed for three modes, respectively. The attenuation is higher

Table 2. Comparison of FEM and experimental frequencies for bare beam.

Mode	Theory (Hz) (closed form)	FEM (Hz) (error)	Experiment (Hz) (error)	Loss factor (experiment)
I	52.05	51.96 (0.17%)	51.00 (1.88%)	0.0060
II	326.20	324.15 (0.60%)	319.00 (1.61%)	0.0065
III	913.40	910.76 (0.3%)	909.10 (2.28%)	0.0073

FEM: finite element method.

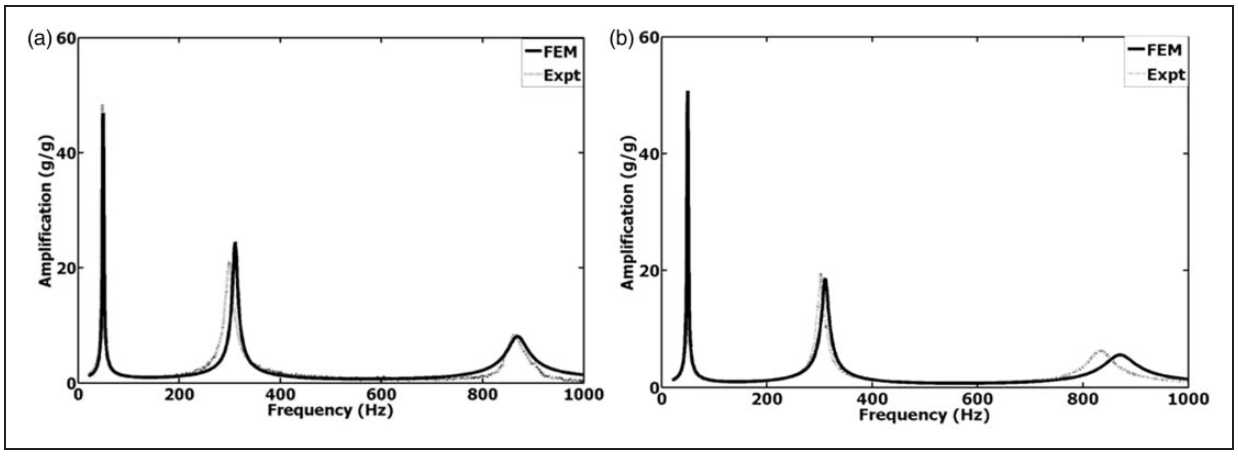

Figure 5. FRF of unconstrained layer sandwich beam of 1 mm thickness: (a) EAP-2 and (b) EAP-43.
FRF: frequency–response function.

for higher modes and EAP-43 shows higher attenuation of amplitudes compared with EAP-2.

Beams with constrained viscoelastic layer sandwich beam (EAP-2 and EAP-43)

From Figure 6(a) and (b), it is seen that the FRF obtained from FE and experiments compare very well for constrained layer of 1 mm thickness for EAP-2 and EAP-43, respectively, and are given in Table 4 along with comparison of loss factors. The results are fairly matching. The error in the experiment is found to be 1%. Attenuations of amplitudes 25, 47 and 56 dB are observed for EAP-2 and 31, 51 and 59 dB are observed for EAP-43. Table 5 gives the overall comparison of amplification factors for bare beam and unconstrained and constrained layer beams for EAP-2 and EAP-43. From the results, it is observed that the attenuation is higher for constrained layer compared with unconstrained layer.

Table 3. Comparison of frequencies and loss factors of unconstrained layer sandwich beam of 1 mm thickness for EAP-2 and EAP-43.

	EAP-2					EAP-43			
	Frequency (Hz)		Loss factors			Frequency (Hz)		Loss factors	
Mode	FEM	Experiment	FEM	Experiment	Mode	FEM	Experiment	FEM	Experiment
I	50.57	49.37	0.0200	0.0214	I	49.50	48.65	0.0218	0.0231
II	310.00	307.00	0.0450	0.0471	II	309.00	302.00	0.0528	0.0546
III	871.00	844.24	0.0797	0.0831	III	869.00	831.00	0.0990	0.1080

FEM: finite element method.

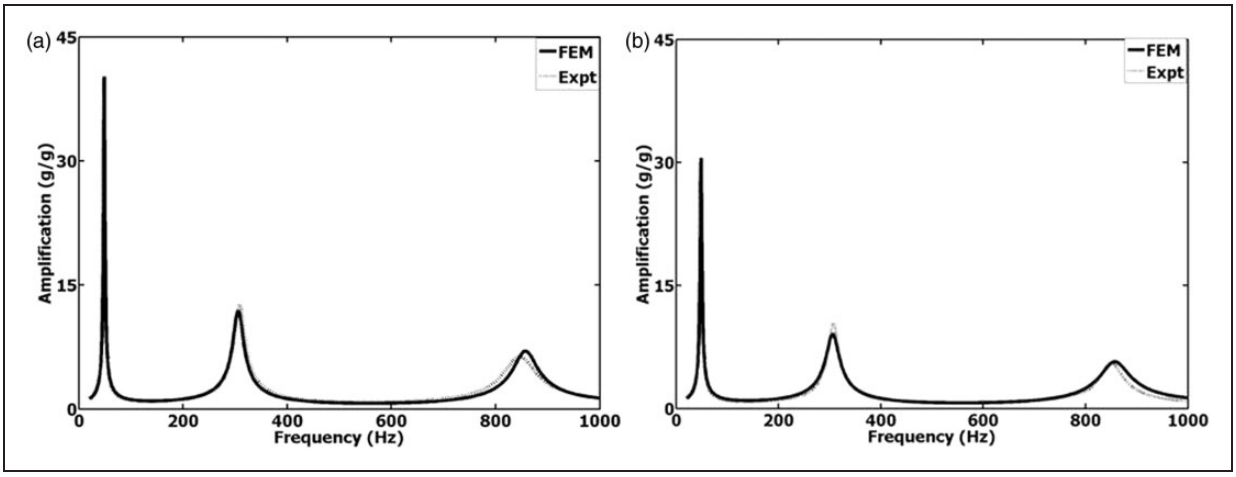

Figure 6. FRF of constrained layer sandwich beam of 1 mm thickness: (a) EAP-2 (b) EAP-43.
FRF: frequency–response function.

Table 4. Comparison of experimental and FE frequencies of constrained layer sandwich beam of 1 mm thickness for EAP-2 and EAP-43.

	EAP-2					EAP-43			
	Frequency (Hz)		Loss factors			Frequency (Hz)		Loss factors	
Mode	FEM	Experiment	FEM	Experiment	Mode	FEM	Experiment	FEM	Experiment
I	48.52	47.37	0.0250	0.0260	I	48.11	47.00	0.0331	0.0340
II	303.07	308.90	0.0730	0.0750	II	307.00	306.00	0.0924	0.0960
III	851.01	847.00	0.1510	0.1580	III	857.00	850.00	0.1820	0.1910

FEM: finite element method.

Table 5. Comparison of amplification factors for EAP-2 and EAP-43 (experimental results).

Amplification, g/g (dB)						
	EAP-2			EAP-43		
	Mode I	Mode II	Mode III	Mode I	Mode II	Mode III
Base beam	139.8 (0)	133.8 (0)	103.3 (0)	139.8 (0)	133.8 (0)	103.3 (0)
Unconstrained layer beam	48.86 (−21)	21.04 (−37)	8.395 (−50)	48.75 (−21)	19.68 (−38)	6.209 (−56)
Constrained layer beam	39.92 (−25)	12.66 (−47)	6.271 (−56)	30.05 (−31)	10.17 (−51)	5.472 (−59)

EAP-43 shows higher attenuation of amplitudes compared with EAP-2.

Conclusions

The frequency-dependent Young's modulus and loss factors expressed in power series for EAP-2 and EAP-43 are introduced in the FE model using iterative scheme. The composite loss factors obtained from FE compared very well with those obtained from experiments. It is observed that the composite loss factors are higher in constrained layer compared with unconstrained layer sandwich. This is due to dissipation of energy being more in shear deformation of constrained layer compared with extension deformation in unconstrained layer beam. The composite loss factor for EAP-43 is higher than that of EAP-2 and this can be attributed to the inter-particle friction and reversible breakage of carbon particle structure on application of strain. The composite loss factors are higher for higher modes in unconstrained and constrained layer beams. The results obtained from constrained layer beam are compared with and without shear effect in the FE model and little improvement was found in the results for thin sandwich beams.

Acknowledgements

The authors are thankful to the Director, Defence Research and Development Laboratory (DRDL), Hyderabad, India, for giving permission to pursue research in the area of layer damping treatment. The viscoelastic material provided by NMRL for evaluating the damping characteristics is greatly acknowledged.

Funding

This research received no specific grant from any funding agency in the public, commercial, or not-for-profit sectors.

References

1. Ross D, Ungar EE and Kerwin EM Jr. Damping of flexural vibrations by means of viscoelastic laminae. In: Ruzicka JE (ed) *Structural damping: colloquium on structural damping,* Sec. III, ASME annual meeting, New York, 1959, pp.49–88.
2. Kerwin Jr EM. Damping of flexural waves by a constrained viscoelastic layer. *J Acoust Soc Am* 1959; 31(7): 952–962.
3. DiTaranto RA. Theory of vibratory bending for elastic and viscoelastic layered finite length beams. *J Appl Mech* 1965; 87: 881–886.
4. Mead DJ and Markus S. The forced vibration of a three-layer damped sandwich beam with arbitrary boundary conditions. *J Sound Vib* 1969; 10(2): 163–175.
5. Mead DJ. Loss factors and resonant frequencies of encastre damped sandwich beams. *J Sound Vib* 1970; 12(1): 99–112.
6. Rao DK. Frequency and loss factors of sandwich beams under various boundary conditions. *J Mech Eng Sci* 1978; 20(5): 271–282.
7. Nakra BC. Vibration control with viscoelastic materials I. *Shock Vib Digest* 1976; 8: 3–12.
8. Nakra BC. Vibration control with viscoelastic materials II. *Shock Vib Digest* 1981; 13: 17–20.
9. Nakra BC. Vibration control with viscoelastic materials III. *Shock Vib Digest* 1984; 16: 17–22.
10. Johnson CD and Kienholz DA. Finite element prediction of damping in structures with constrained viscoelastic layers. *AIAA J* 1982; 20(9): 1284–1290.
11. Golla DF and Hughes PC. Dynamics of viscoelastic structures – a time domain finite element formulation. *J Appl Mech* 1985; 52(4): 897–906.
12. McTavish DJ and Hughes PC. Modeling of linear viscoelastic space structures. *J Vib Acoust* 1993; 115: 103–110.
13. Lesieutre GA and Bianchini E. Time domain modeling of linear viscoelasticity using anelastic displacement fields. *J Vib Acoust* 1995; 117: 424–430.
14. Torvik PJ and Runyon BD. Estimating the loss factors of plates with constrained layer damping treatments. *AIAA J* 2007; 45(7): 1492–1500.
15. Cortes F and Elejabarrieta MJ. Structural vibration of flexural beams with thick unconstrained layer damping. *Int J Solid Struct* 2008; 45: 5805–5813.
16. Barbosa FS and Farage MCR. A finite element model for sandwich viscoelastic beams: experimental and numerical assessment. *J Sound Vib* 2008; 317: 91–111.
17. Amichi K and Atalla N. A new 3D finite element for sandwich beams with a viscoelastic core. *J Vib Acoust* 2009; 131(2): 3930–3943.
18. Navin Kumar and Singh SP. Vibration and damping characteristics of beams with active constrained layer under parametric variations. *Mater Des* 2009; 30: 4162–4174.
19. Bangarubabu P, Kishore Kumar K and Krishna Y. Damping effect of viscoelastic material on sandwich beams. In: *International conference on trends in industrial and mechanical engineering (ICTIME 2012)*, Dubai, 24–25 March 2012, pp.171–173.

20. Mead DJ. *Passive vibration control*. England, UK: John Wiley and Sons, 1988.
21. Gawronski WK. *Advanced structural dynamics and active control of structures*. New York: Springer-Verlag, 2004 Chapters 2–3.
22. Torvik PJ. On estimating system damping from frequency response bandwidths. *J Sound Vib* 2011; 330: 6088–6097.

Appendix

Notation

A,B, C, D	system state representation
$E^*(f)$	complex Young's modulus of VEM
$E^v(f)$	Young's modulus of viscoelastic material
f	frequency (Hz)
$[H_m(s)]$	modal transfer function
H(s)	transfer function
$[H(s)]_i$	transfer function at i_{th} location
$H(\omega)$	frequency response function
$[K^*]$	complex stiffness matrix of viscoelastic layer
$[k^e]^*_{eq}$	element stiffness matrix of sandwich beam
$[K^I]$	imaginary part of complex stiffness matrix
$[K^R]$	real part of complex stiffness matrix
L_e	length of beam element
m	modal
m_e	mass per unit length of sandwich beam
$[m^e]_{eq}$	element mass matrix of sandwich beam
[M],[K] and [C]	global mass, damping and stiffness matrices
[P]	modal matrix
$\{q_m\}$	modal response vector
s	Laplace domain
W	transverse displacement
z	state vector
$\eta(f)$	loss factor of viscoelastic material